AEROMECHANICAL ANALYSIS OF A COMPLETE WIND TURBINE USING NONLINEAR FREQUENCY DOMAIN SOLUTION METHOD

Shine Win Naung[1], Mohammad Rahmati[*1], Hamed Farokhi[1]

[1]Department of Mechanical and Construction Engineering, Faculty of Engineering and Environment, Northumbria University, Newcastle upon Tyne, United Kingdom, NE1 8ST

[*]Corresponding author

Email: mohammad.rahmati@northumbria.ac.uk

ABSTRACT

The high-fidelity computational fluid dynamics (CFD) simulations of a complete wind turbine model usually require significant computational resources. It will require much more resources if the fluid-structure interactions between the blade and the flow are considered, and it has been the major challenge in the industry. The aeromechanical analysis of a complete wind turbine model using a high-fidelity CFD method is discussed in this paper. The distinctiveness of this paper is the application of the nonlinear frequency domain solution method to analyse the forced response and flutter instability of the blade as well as to investigate the unsteady flow field across the wind turbine rotor and the tower. This method also enables the aeromechanical simulations of wind turbines for various inter blade phase angles in a combination with a phase shift solution method. Extensive validations of the nonlinear frequency domain solution method against the conventional time domain solution method reveal that the proposed frequency domain solution method can reduce the computational cost by one to two orders of magnitude.

Keywords: wind turbines; aerodynamics; aeroelasticity; computational fluid dynamics; nonlinear frequency domain solution method

1. INTRODUCTION

The power generation from renewable energy resources has been significantly increased in recent years. Among renewable energy resources, wind power is one of the fastest-growing technologies due to its promising advantages. A lot of research has been done over the last decade to produce energy from the wind more effectively and efficiently. Due to recent technical advances, the sizes of wind turbine blades are getting larger and longer over the past years, which could potentially introduce aeroelastic instabilities such as blade flutter leading to several catastrophic structural failures [1]. Therefore, it is vital to explore and understand the aeroelastic instability problems of wind turbines.

The aeroelastic instabilities of wind turbines are typically triggered by the interaction between the fluid flow and the blade structure. Thus, a Fluid-Structure Interaction (FSI) method must be considered to understand the aeroelasticity. Blade Element Momentum (BEM) theory has traditionally been adopted in wind turbine simulations [2]. Lin et al. [3] used the BEM theory and mixed-form formulation of Geometrically Exact Beam Theory (GEBT) to study the nonlinear aeroelastic modelling for wind turbine blades. Fernandez et al. [4] proposed a methodology for the aero-structural analysis of a wind turbine blade using BEM and Finite Element (FE) models. Likewise, Rafiee et al. [5] conducted the aeroelasticity analysis of a wind turbine blade coupling the BEM method and the FE method. In these studies, the aerodynamic loads are obtained from BEM models. However, the BEM models are unable to accurately capture the nature of flow behaviour resulting in a lack of confidence to understand the aerodynamics of wind turbines.

The vortex models using prescribed-wake methods or free-wake methods are also used in the research industry to study aerodynamics and aeroelasticity of wind turbines or aircrafts. A study performed by Palacios et al. [6] proposed and concluded that the Unsteady Vortex-Lattice Method (UVLM) can be used, as an alternative to the high-fidelity methods, for aerodynamic modelling with coupled aeroelasticity and flight dynamics, considering the effects associated with geometric nonlinearities. Riziotis et al. [7] and Min-Soo Jeong et al. [8] employed a free-wake model to analyse the aerodynamic and aeroelastic behaviour of wind turbine blades under different conditions. Not only that the viscous effects are neglected in most vortex models, which results in a limited understanding of the aeroelasticity of wind turbine, but also they require more computational resources compared to BEM models. Hence, the use of a high-fidelity numerical model at an affordable computational cost is required for the wind energy research industry.

Computational Fluid Dynamics (CFD) methods, either using Reynolds Averaged Navier-Stokes (RANS) equations for steady simulations or Unsteady Reynolds Averaged Navier-Stokes (URANS) equations for unsteady simulations, are capable of modelling and capturing detailed flow behaviours and they have been widely used in the industry for wind turbine applications. Typically, the CFD methods are computationally expensive and require large computational resources [9-10]. Kaya et al. [11] used a CFD method to investigate the aerodynamic performance of a wind turbine with forward and backward swept blades. Lin et al. [12] proposed an FSI modelling method for the wind turbine blade using CFD and FE models and calculated its structural responses such as stress distribution and blade tip deflections using different wind loads. However, they are based on RANS models. Dong et al. [13] developed a coupled CFD and Computational Structural Dynamics (CSD) method based on the URANS model to predict aerodynamic loads applied on the wind turbine blade and its time-varying aeroelastic responses. Similarly, Dai et al. [14] analysed the aeroelastic performance of wind turbine blades subject to different yaw conditions using the URANS model and the FE model.

Usually, the unsteady simulations using URANS models are computationally expensive depending on the size of the computational domain and the numerical method used. Seeking efficient numerical methods, which could reduce the computation time without compromising the required accuracy, has been the main interest in the research industry. He et al. [15] and Hall et al. [16] developed a time-linearized harmonic frequency-domain method for the calculation and analysis of unsteady flows in turbomachinery. This method was later replaced by the harmonic balance method of Hall et al. [17], the phase solution method of He [18], and Rahmati et al. [19-20] due to their capability of modelling flow nonlinearity and harmonic disturbances. These methods have been widely used in turbomachinery. Rahmati et al. [21-22] also developed a nonlinear frequency domain method for the multi-row aeromechanical analysis of turbomachines and showed that a fully coupled multi-row configuration should be considered rather than a simplified isolated one to produce better accuracy in predicting flutter behaviour of the blades. Despite the fact that the frequency domain methods are typically used in turbomachinery analysis, there are only a few recently conducted studies in the field of wind turbine research which employ such methods [23-26].

The frequency domain solution method is proposed and employed in this paper to study the aeroelasticity of a complete wind turbine model and to investigate the unsteady flow field around the wind turbine. The proposed frequency domain solution method is validated against the conventional time domain solution method. A test case wind turbine, the MEXICO (Model Rotor Experiments In Controlled Conditions) Experiment wind turbine, is selected for this study. This paper can be considered as a continuation of the authors' previous studies [27-28] in which the aerodynamic and aeromechanical simulations of wind turbine rotors are presented using a frequency domain method.

2. METHODOLOGY

2.1 Flow Governing Equations

In the present work, a three-dimensional density-based finite volume solver is employed for the flow computation. The simulations are performed based on the URANS model. The flow is governed by the Navier-Stokes equations and it can be expressed as:

$$\frac{\partial}{\partial t}\int_{\Omega} U d\Omega + \int_{S} \vec{F}_I \,.d\vec{S} + \int_{S} \vec{F}_V \,.d\vec{S} = \int_{\Omega} S_T d\Omega \qquad (1)$$

where Ω is the volume, S is the surface, U is the vector of the conservative variables, S_T is the source term, and $\vec{F}_I$and $\vec{F}_V$are the inviscid and viscous flux vectors, respectively. Spalart–Allmaras turbulence model is employed in this work and the above equation can be simply written in a semi-discrete form as [19-22]:

$$\frac{\partial}{\partial t}(U) = R(U) \quad (2)$$

where R is the lumped residual and the source term. A central scheme and a four-stage explicit Runge–Kutta scheme are used for spatial and temporal discretization, respectively.

2.2 Frequency Domain Solution Method

In wind turbine aerodynamics and aeroelasticity, the unsteadiness of the flow can be associated with the blade deflection. The unsteady terms corresponding to the flow unsteadiness can be represented by a Fourier series for a prescribed fundamental frequency, ω, and the specified number of harmonics, m, as expressed in Eq. (3).

$$U = \bar{U} + \sum_{m=1}^{M}[A_U \sin(m\omega t) + B_U \cos(m\omega t)] \quad (3)$$

where $\bar{U}$, A_U, and B_U are the Fourier coefficients of the conservation variables. The accuracy of the unsteady solution can be controlled through the order of the Fourier series. The unsteady period is equally divided into $N = (2m+1)$ time levels and the system of nonlinear equations coupling all N time levels are solved iteratively. The fundamental mode (one harmonic) is enough for this study, and the flow solution with one harmonic is given by:

$$U = \bar{U} + A_U \sin(\omega t) + B_U \cos(\omega t) \quad (4)$$

Substituting Eq. (4) into Eq. (2) yields the following equation:

$$\omega(A_U \cos(\omega t) - B_U \sin(\omega t)) = R \quad (5)$$

At three distinctive temporal phases, Eq. (4) can be written as follows:

$$U_0 = \bar{U} + B_U \qquad \omega t = 0 \quad (6.a)$$

$$U_{\pi/2} = \bar{U} + A_U \qquad \omega t = \pi/2 \quad (6.b)$$

$$U_{-\pi/2} = \bar{U} - A_U \qquad \omega t = -\pi/2 \quad (6.c)$$

These three equations can be used to compute the three Fourier coefficients, $\bar{U}$, A_U, and B_U. Expressing these coefficients in terms of the flow solutions at the three phases and substituting into Eq. (5) yields the following equations:

$$\omega\left(\frac{U_{\pi/2}-U_{-\pi/2}}{2}\right)-R_0=0 \tag{7.a}$$

$$\omega\left(U_0-\frac{U_{\pi/2}+U_{-\pi/2}}{2}\right)+R_{\pi/2}=0 \tag{7.b}$$

$$\omega\left(U_0-\frac{U_{\pi/2}+U_{-\pi/2}}{2}\right)-R_{-\pi/2}=0 \tag{7.c}$$

These three sets of equations are simultaneously solved in a similar way to that of the steady RANS equations with the extra term being treated as a source term. A pseudo time derivative term is added to the three sets of equations so that the Runge–Kutta method can be used to time-march their solutions to a steady-state [19-22].

2.3 Fluid-Structure Interaction

The modal coupling FSI method, which adopts the CFD method for the aerodynamic calculation and the FE method for the structural calculation, is implemented in this paper.

The solid mechanics of a structure is governed by the following equation:

$$[M]\frac{\partial^2\vec{d}}{\partial t^2}+[C]\frac{\partial\vec{d}}{\partial t}+[K]\vec{d}=\vec{f} \tag{8}$$

where $[M]$ is the mass matrix, $[C]$ is the damping matrix, $[K]$ is the stiffness matrix, $\vec{d}$ is the displacement of the structure, and $\vec{f}$ is the external load.

The global displacement of the structure can be written as:

$$\vec{d}=\sum_{i=1}^{n_{modes}} q_i\vec{\phi}_i \tag{9}$$

where q_i is the generalized displacement and $\vec{\phi}_i$ is the natural mode shapes of the structure normalized by the mass.

Substituting Eq. (9) into Eq. (8) and multiplying with $\vec{\phi}_i^{\,T}$ yields the following equation:

$$\frac{d^2q_i}{dt^2}+2\xi_i\omega_i\frac{dq_i}{dt}+\omega_i^2q_i=\vec{\phi}_i^{\,T}\vec{f} \tag{10}$$

where ω_i is the natural frequencies of the structure and ξ_i is the damping coefficient.

For the modal coupling method, a structure code is used to compute the modal shapes and the natural frequencies of the structure prior to the flow simulation. The generalized displacement q_i needs to be specified for the considered amplitude of deformation and it can be written as:

$$q_i(t) = \bar{q} + q_A \cos(\omega_i t) \tag{11}$$

where $\bar{q}$ and q_A are the mean value and amplitude of the displacement, respectively. Having this information, the flow solver computes the deformation of the structure by solving Eq. (9).

2.4 Boundary Conditions

The solid wall boundary condition is applied on the blade, the hub and the tower. The external boundary condition, which is a non-periodic one, is defined to treat the far-field boundaries dealing with the external flow computations. A rotor-stator interface connecting the rotor side of the grid and the tower side of the grid is introduced to simulate a complete wind turbine model. For the periodic boundaries of the rotor, the direct periodic (repeating) condition is applied for the time domain method whereas only a single passage domain is required for the frequency domain solution method. With the frequency domain method, the harmonic components are phase-shifted between the periodic boundaries by a given Inter Blade Phase Angle (IBPA), σ, as expressed in the following equations [19-22] where the subscript 1 and 2 are corresponding to the referenced passage and its neighbouring one, respectively.

$$A_{U,2} = A_{U,1} \cos(\sigma) - B_{U,1} \sin(\sigma) \tag{12.a}$$

$$B_{U,2} = A_{U,1} \sin(\sigma) + B_{U,1} \cos(\sigma) \tag{12.b}$$

3. THE MEXICO-EXPERIMENT WIND TURBINE

The MEXICO Experiment was conducted in a wind tunnel in the Large-Scale Low-Speed Facility of the German-Dutch Wind Tunnel (DNW) [29-32]. Numerical simulations have also been carried out for this wind turbine [33-37]. The selected parameters of this wind turbine which are used in the present simulations are listed in Table 1, and further details can be found in the authors' previous papers [27-28]. The modal coupling FSI method, as described in the methodology section, is used to conduct the aeromechanical analysis. To the best of the authors' knowledge, this type of analysis is conducted for the first time for this wind turbine including the tower. The frequency domain method is applied to this analysis. As the experiment for the aeromechanical analysis is always difficult to be performed and no experimental data for such analysis are available for this wind turbine, the

conventional time domain solution method is used for validation purposes. The Aluminium Alloy is used for the material of the blade to be similar to the one used in the experiment. It has a density of 2770 kg/m^3, Young's modulus of 7.1E+10 Pa, and the Poisson ratio of 0.27.

4. COMPUTATIONAL DOMAIN AND GRID

A structured grid generator is used to generate a three-dimensional computational domain and grid. In order to simulate the complete wind turbine model, the rotor side and the tower side are meshed separately, and they are connected through a rotor-stator interface. A Rounded Azimuthal O4H topology is used for the generation of both rotor and tower grids. Each grid consists of five blocks such as the skin block surrounding the blade, the inlet block located upstream of the leading edge, the outlet block located downstream of the trailing edge, the upper block located above the blade section, and the lower block located under the blade section. An O-mesh is used for the skin block whereas an H-mesh is used for the remaining blocks. With the frequency domain solution method, only a single passage of the rotor is required whereas a full passage domain (360 degrees) including three blades is used for the time domain solution method. A 360 degrees grid is generated for the tower side. The flow inlet and outlet are located 2R upstream of the rotor and 4R downstream of the rotor, respectively, and the far-field boundary is placed 3R from the origin of coordinates, where R is the rotor radius. There are studies in the literature which used similar domain sizes and showed that they can accurately predict the blade loading and flow behaviour [12,26,38]. Therefore, it can be noted that the considered distances for far-field boundaries are sufficiently far away from the turbine. The first cell layer thickness is 1e-5 meters to ensure that the y^+ value is less than one. A single passage of the rotor side of the grid has 4.5 million grid points and the tower side of the grid has 9 million grid points. A grid sensitivity study is also carried out to ensure that the grid size is suitable for this study. Figure 1 presents the differences in computing the blade loads such as torque with respect to the combined rotor and tower grid size. As seen, less than one percent improvement is obtained beyond 13 million grid points. Thus, the grid size used in this study can be considered suitable for the present work. The generated computational domain and grid is shown in Fig. 2.

5. RESULTS

First of all, the steady pressure coefficient distributions computed from this work are compared to the experiment as well as the previous simulation performed by Sorensen et al. [34] for the validation of the CFD model. Figure 3 shows the comparison of the steady pressure coefficient distributions at 25%, 35%, 60%, 82% and 92% span blade sections. Slight differences in predicting pressure distribution are seen between the experiment and the CFD simulations at the 25% and 35% blade span sections. However, they are due to instability in the pressure transducers during the experiment as discussed in [33-34]. Overall, the present simulation results are very close to those of Sorensen et al. [34] and they are in good agreement with the experiment.

Using the validated numerical model, the aeromechanical analysis of the MEXICO-Experiment wind turbine including the tower is performed. The natural frequencies and mode shapes of the blade are first computed through the modal analysis before the flow

simulation. For the blade vibration, the first vibration mode is used with the first natural frequency, 15.611 Hz, as the vibration frequency and the maximum vibration amplitude is 2% of the blade span. The IBPA for this simulation is defined to be 120 degrees. The frequency domain method combining with the phase shift method is used for this analysis. It is understood that the experimental data for this analysis are not available and thus, the frequency domain method is validated against the time domain method. The time domain solution is performed using 20 time-steps per vibration period with 100 inner iterations per time-step, and it is solved over several vibration cycles until a steady-periodic state is reached.

Unsteady pressure distribution due to the blade deflection can be divided into the time-averaged value and amplitude of fluctuation as described in Eq. (4), and it can be written as:

$$P = \bar{P} + P_A \sin(\omega t) + P_B \cos(\omega t) \tag{13}$$

where $\bar{P}$ is the time-averaged pressure, and P_A and P_B are Fourier coefficients. The unsteady pressure amplitude can be defined as $\sqrt{{P_A}^2 + {P_B}^2}$. Figures 4-6 present the comparison of the time-averaged pressure coefficient and unsteady pressure amplitude coefficient distributions at three blade sections computed from the time domain method and the frequency domain method. As seen, they are in good agreement. This ensures that the frequency domain method can be used for the calculation of unsteady pressure distributions associated with the blade deflection. Furthermore, Fig. 7 illustrates the pressure coefficient profiles along an axis parallel to the rotation axis, located at the blade mid-span, from one rotor diameter upstream to one rotor diameter downstream of the rotor plane, obtained from both time domain and frequency domain methods. As shown, both methods predicted the similar pressure distribution across the rotor and the tower including a little pressure disturbance occurred due to the presence of the tower.

In addition to the pressure coefficients, the skin friction coefficients at 30% and 90% of the blade span sections are compared between the time domain method and the frequency domain method, and they are shown in Fig. 8. As shown, they agree well with each other. Good agreements between the two methods are also obtained at other sections but they are not shown in this paper. Figure 9 demonstrates blade loads such as torque and axial thrust profiles as well as the aerodynamic power profile for one rotor revolution computed from both time domain and frequency domain methods. It is seen that these profiles are associated with the blade vibration frequency, and the results obtained are in good agreement.

The aerodynamic damping value, calculated from the aerodynamic work per vibration cycle, is typically used in the turbomachinery analysis to investigate whether the blade structure vibration can lead to the flutter phenomena. The aerodynamic damping is evaluated using both methods and they are listed in Table 2. As shown, they are close to each other. The aerodynamic damping is positive which shows that the fluid damps the blade structure vibration. The blade displacement contour and

displacement profiles for one rotor revolution are presented in Fig. 10 and 11, respectively, which demonstrate that each blade vibrates out of phase with respect to the others by a phase angle of 120 degrees. Only a single passage domain is required for this analysis with the frequency domain method whereas a 360 degrees rotor domain including all three blades is required for the time domain method resulting in much more computation time.

As the tower is present in the present simulation, it is also required to analyse the effects associated with the tower. Figure 12 demonstrates the velocity flow fields on a plane normal to the wind direction, extracted just behind the rotor, at the middle between the rotor and the tower, and just before the tower, to visualise the behaviour of the flow interaction with the rotor and the tower. As shown in Fig. 12 (a), the high velocity is built-up along the leading edge of the blade as the blade rotates generating the blade tip vortex as well as leaving the lower velocity field behind the trailing edge. In Fig. 12 (b), the high-velocity field moves a little farther away from the blade tip. This process can be identified as the wake expansion process. As the flow approaches the tower, the flow is disturbed by the tower structure resulting in the high-velocity field on each side of the tower as well as the flow separation and recirculation behind the tower (see Fig. 12 (c)). The interaction between the unsteady flow field and the tower can also be better visualised in the meridional view, as illustrated in Fig. 13. It is seen that the flow is highly distorted by the tower structure, and the flow separation and recirculation are observed behind the tower, leading to further unsteadiness and instability in the downstream wake. It should be noted that the images from Fig. 12 and 13 are obtained from the time reconstruction of the frequency domain solution. The images from the time domain solution are not shown as they are very similar.

The simulations discussed in this paper are performed on a single CPU with a 3.40 GHz Intel (R) Core (TM) i5-7500 CPU. With the time domain method, it requires much more CPU time as the full domain with all three blades is used in the simulation whereas only a single passage domain of the rotor is required for the frequency domain method. In terms of computation time, it takes 17 hours using the frequency domain method. However, it takes 10 days on the same computer if the time domain method is used.

6. CONCLUSIONS

The aeromechanical analysis of a complete wind turbine model including the tower is presented in this paper. A test case wind turbine, the MEXICO-Experiment wind turbine, is selected for this study. The CFD model used in this work is first validated against the experiment as well as the reference CFD simulation, and the results obtained are in good agreement. The aeromechanical simulation of this wind turbine is then conducted using the validated CFD model. The frequency domain solution method in a combination with the phase shift method is applied to this investigation. The time domain method is adopted to validate the frequency domain method due to the lack of experimental data. The time-averaged pressure and unsteady pressure amplitude coefficients at different blade sections are computed and compared between the two methods, and results agree well with each other. The pressure profile across the rotor and the tower is also calculated and both methods predicted similar pressure distributions. In

addition, the skin friction coefficients at different blade sections, blade loads such as torque and axial thrust profiles as well as the aerodynamic power profile for one rotor revolution are computed, and the results are compared between the two methods. Likewise, they are in very good agreement. The stability of the blade vibration is also examined in this study computing the aerodynamic damping value. It is shown that the blade vibration is damped and the aerodynamic damping values predicted from both methods are close to each other. Flow visualisations in terms of velocity magnitude indicate that the flow is distorted by the tower and the flow interaction with the tower results in further unsteadiness and instability in the downstream wake.

The comparison of the computational cost shows that the frequency domain solution method is much faster than the time domain solution method, and the computation time can be reduced by one to two orders of magnitude using the frequency domain solution method. In conclusion, the frequency domain solution method can be reliably used for the aeromechanical analysis of complete wind turbine models for any IBPA values saving computation time significantly.

ACKNOWLEDGEMENTS

The authors would like to acknowledge the financial support received from the Engineering Physics and Science Research Council of the UK (EPSRC EP/R010633/1).

REFERENCES

[1] Hansen, M.H., 2007, “Aeroelastic Instability Problems for Wind Turbines,” Wind Energy, 10, pp. 551–577.

[2] Wang, Q., Wang, J., Chen, J., Luo, S., and Sun, J., 2015, “Aerodynamic shape optimized design for wind turbine blade using new airfoil series,” Journal of Mechanical Science and Technology, 29 (7), pp. 2871-2882.

[3] Wang, L., Liu, X., Renevier, N., Stables, M., and Hall, G.M., 2014, “Nonlinear aeroelastic modelling for wind turbine blades based on blade element momentum theory and geometrically exact beam theory,” Energy, 76, pp. 487-501.

[4] Fernandez, G., Usabiag, H., and Vandepit, D., 2018, “An efficient procedure for the calculation of the stress distribution in a wind turbine blade under aerodynamic loads,” Journal of Wind Engineering & Industrial Aerodynamics, 172, pp. 42–54.

[5] Rafiee, R., Tahani, M., and Moradi, M., 2016, “Simulation of aeroelastic behavior in a composite wind turbine blade,” Journal of Wind Engineering & Industrial Aerodynamics, 15, pp. 60–69.

[6] Murua, J., Palacios, R., and Graham, J.M.R., 2012, “Applications of the unsteady vortex-lattice method in aircraft aeroelasticity and flight dynamics,” Progress in Aerospace Sciences, 55, pp. 46–72.

[7] Riziotis, V.A., Manolas, D.I., and Voutsinas, S.G., 2011, “Free-wake Aeroelastic Modelling of Swept Rotor Blades,” Conference: EWEA, Brussels, Belgium.

[8] Jeong, M.S., Kim, S.W., Lee, I., Yoo, S.J., and Park, K.C., 2013, “The impact of yaw error on aeroelastic characteristics of a horizontal axis wind turbine blade,” Renewable Energy, 60, pp. 256-268.

[9] Wang, L., Liu, X., and Kolios, A., 2016, “State of the art in the aero-elasticity of wind turbine blades: Aero-elastic modelling,” Renewable and Sustainable Energy Review, 64, pp. 195–210.

[10] O'Brien, J.M., Young, T.M., O'Mahoney, D.C., and Griffin, P.C., 2017, “Horizontal axis wind turbine research: A review of commercial CFD, FE codes and experimental practices,” Progress in Aerospace Sciences, 92, pp. 1–24.

[11] Kaya, M.N., Kose, F., Ingham, D., Ma, L., and Pourkashanian, M., 2018, “Aerodynamic performance of a horizontal axis wind turbine with forward and backward swept blades,” Journal of Wind Engineering & Industrial Aerodynamics, 176, pp. 166–173.

[12] Wang, L., Quant, R., and Kolios, A., 2016, “Fluid structure interaction modelling of horizontal-axis wind turbine blades based on CFD and FEA,” Journal of Wind Engineering & Industrial Aerodynamics, 158, pp. 11-25.

[13] Yu, D.O., and Kwon, O.J., 2014, “Predicting wind turbine blade loads and aeroelastic response using a coupled CFD-CSD method,” Renewable Energy, 70, pp. 184-196.

[14] Dai, L., Zhou, Q., Zhang, Y., Yao, S., Kang, S., and Wang, X., 2017, “Analysis of wind turbine blades aeroelastic performance under yaw conditions,” Journal of Wind Engineering & Industrial Aerodynamics, 171, pp. 273–287.

[15] He, L., and Ning, W., 1998, “An Efficient Approach for Analysis of Unsteady Viscous Flows in Turbomachines,” AIAA J., 36 (11), pp. 2005–2012.

[16] Hall, K., and Lorence, C., 1993, “Calculation of Three-Dimensional Unsteady Flows in Turbomachinery Using the Linearized Harmonic Euler Equations,” ASME J Turbomach., 115(4), pp. 800–809.

[17] Hall, K., Thomas, J., and Clark, W., 2002, “Computation of Unsteady Nonlinear Flows in Cascades Using a Harmonic Balance Technique,” AIAA J., 40(5), pp. 879–886.

[18] He, L., 2008, “Harmonic Solution of Unsteady Flow Around Blades With Separation,” AIAA J., 46(6), pp. 1299–1307.

[19] Rahmati, M.T., He, L., and Wells, R.G., 2010, “Interface treatment for harmonic solution in multi-row aeromechanic analysis,” Proceedings of ASME Turbo Expo 2010: Power for Land, Sea, and Air, Glasgow, UK, June 14-18, 2010.

[20] Rahmati, M.T., He, L., and Li, Y.S., 2012, “Multi-row interference effects on blade aeromechanics in compressor and turbine stages,” 13th International Symposium on Unsteady Aerodynamics, Aeroacoustics and Aeroelasticity of Turbomachines (ISUAAAT), Tokyo, Japan, September 11-14, 2012.

[21] Rahmati, M.T., He, L., and Li, Y.S., 2015, “The Blade Profile Orientations Effects on the Aeromechanics of Multirow Turbomachines,” ASME J Eng. Gas. Turb. Power., 138(6), 062606.

[22] Rahmati, M.T., He, L., Wang, D.X., Li, Y.S., Wells, R.G., and Krishnababu, S.K., 2014, “Nonlinear Time and Frequency Domain Method for Multi-Row Aeromechanical Analysis,” ASME J Turbomach., 136(4), 041010.

[23] Howison, J., Thomas, J., and Ekici, K., 2018, “Aeroelastic analysis of a wind turbine blade using the harmonic balance method,” Wind Energy, 21, pp. 226–241.

[24] Drofelnik, J., Ronch, A.D., and Campobasso, M.S., 2018, “Harmonic balance Navier-Stokes aerodynamic analysis of horizontal axis wind turbines in yawed wind,” Wind Energy, 21, pp. 515–530.

[25] Harcas, S.G., Debrabandere, F., Tartinville, B., Hirsch, C., and Coussement, G., 2017, "Rotor-tower interactions of DTU 10MW reference wind turbine with a non-linear harmonic method," Wind Energy, 20, pp. 619–636.

[26] Horcas, S.G., Debrabandere, F., Tartinville, B., Hirsch, C., and Coussement, G., 2017, "Extension of the Non-Linear Harmonic method for the study of the dynamic aeroelasticity of horizontal axis wind turbines," Journal of Fluids and Structures, 73, pp. 100–124.

[27] Win Naung, S., Rahmati, M.T., and Farokhi, H., 2019, "Aerodynamic Analysis of a Wind Turbine with Elevated Inflow Turbulence and Wake using Harmonic Method," Proceedings of the ASME 2019 38th International Conference on Ocean, Offshore and Arctic Engineering (OMAE2019), Glasgow, Scotland, June 9-14, 2019.

[28] Win Naung, S., Rahmati, M.T., and Farokhi, H., 2019, "Aeromechanical Analysis of Wind Turbines using Non-linear Harmonic Method," Proceedings of the ASME 2019 38th International Conference on Ocean, Offshore and Arctic Engineering (OMAE2019), Glasgow, Scotland, June 9-14, 2019.

[29] Schepers, J.G., Pascal, L., and Snel, H., 2010, "First results from Mexnext: Analysis of detailed aerodynamic measurements on a 4.5 m diameter rotor placed in the large German Dutch Wind Tunnel DNW," The European Wind Energy Conference and Exhibition (EWEC), Warsaw, Poland, April 20-23, 2010.

[30] Schepers, J.G., Boorsma, K., and Munduate, X., 2012, "Final Results from Mexnext-I: Analysis of detailed aerodynamic measurements on a 4.5 m diameter rotor placed in the large German Dutch Wind Tunnel DNW," The Science of making Torque, Oldenburg, Germany, October 9-11, 2012.

[31] Schepers, J.G., and Snel, H., 2007, "Model Experiments in Controlled Conditions, Final report," ECN-E-07-042, ECN.

[32] Schepers, J.G., Boorsma, K., Kim, C., and Cho, T., 2012, "Final report of IEA Task 29, Mexnext (Phase 1): Analysis of Mexico wind tunnel Measurements," ECN-E–12-004, ECN.

[33] Carrion, M., Woodgate, M., Steijl, R., and Barakos, G., 2014, "CFD and Aeroelastic Analysis of the MEXICO Wind Turbine," Journal of Physics. Conf. Ser., 555 012006.

[34] Bechmann, A., Sørensen, N.N., and Zahle, F., 2011, "CFD simulations of the MEXICO rotor," Wind Energy, 14, pp. 677–689.

[35] Sørensen, N.N., Zahle, F., Boorsma, K., and Schepers, G., 2016, "CFD computations of the second round of MEXICO rotor measurements," Journal of Physics. Conf. Ser., 753 022054.

[36] Herraez, I., Medjroubi, W., Stoevesandt, B., and Peinke, J., 2014, "Aerodynamic Simulation of the MEXICO Rotor," Journal of Physics. Conf. Ser., 555 012051.

[37] Plaza, B., Bardera, R., and Visiedo, S., 2015, "Comparison of BEM and CFD results for MEXICO rotor aerodynamics," Journal of Wind Engineering & Industrial Aerodynamics, 145, pp. 115–122.

[38] Martinez, J., Doerffer, P., Szulc, O., and Tejero, F., 2015, "Aerodynamic Analysis of Wind Turbine Rotor Blades," TASK QUARTERLY, 19(2), pp. 129-140.

TABLE 1: PARAMETERS OF THE MEXICO-EXPERIMENT WIND TURBINE

Number of Blades	3
Blade Length	2.04 [m]
Rotor Diameter	4.5 [m]
Design Wind Speed	15 [m/s]
Rotational Speed	424.5 [RPM]
Design Pitch Angle	-2.3 [deg]

TABLE 2: AERODYNAMIC DAMPING

Method	**Aerodynamic Damping**
Frequency Domain Solution Method	0.25
Time Domain Solution Method	0.26

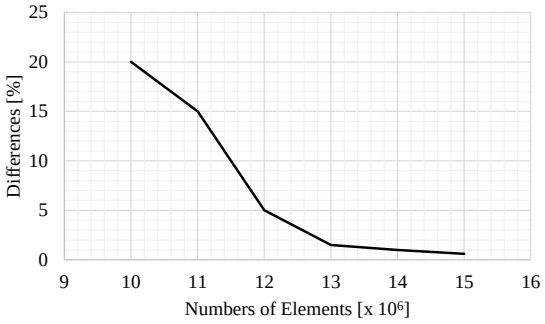

FIGURE 1: GRID SENSITIVITY STUD

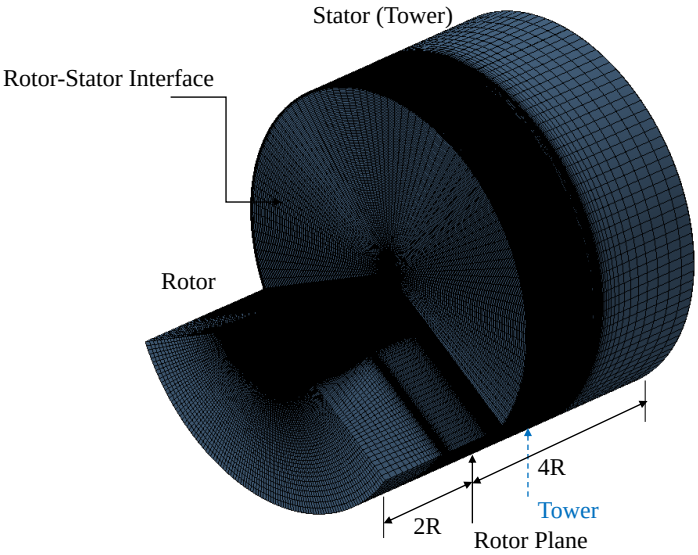

(a)

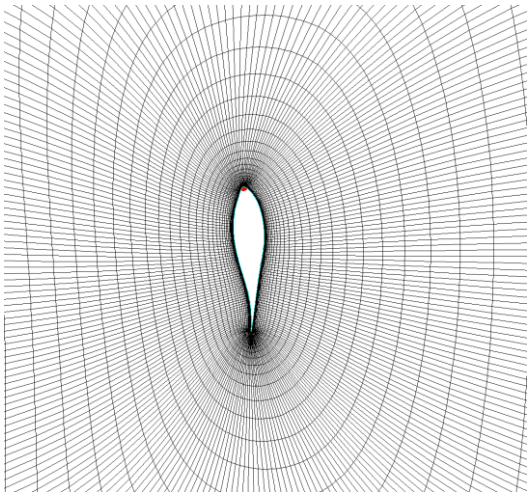

B2B Mesh

(b)

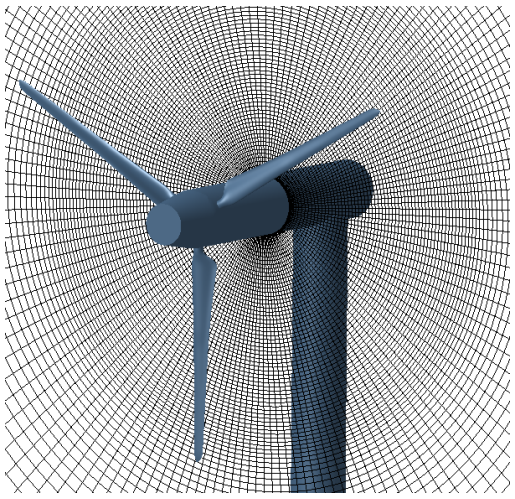

Rotor-Stator Interface

(c)

FIGURE 2: (A) COMPUTATIONAL DOMAIN AND GRID, (B) BLADE-TO-BLADE VIEW OF THE MESH, AND (C) ROTOR-STATOR INTERFACE OF THE MEXICO-EXPERIMENT WIND TURBINE

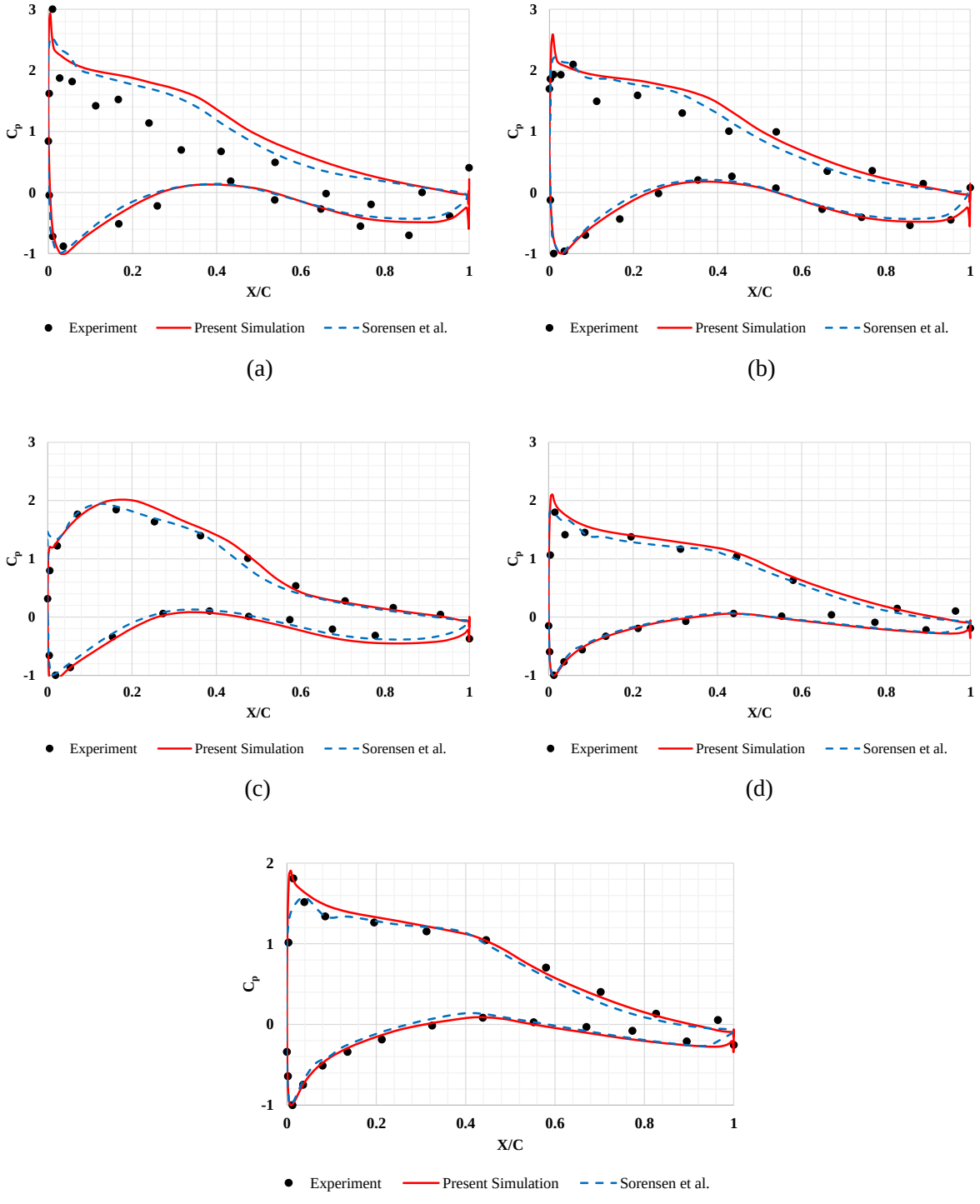

FIGURE 3: STEADY PRESSURE COEFFICIENT DISTRIBUTIONS AT (A) 25%, (B) 35%, (C) 60%, (D) 82%, AND (E) 92% OF THE BLADE SPAN

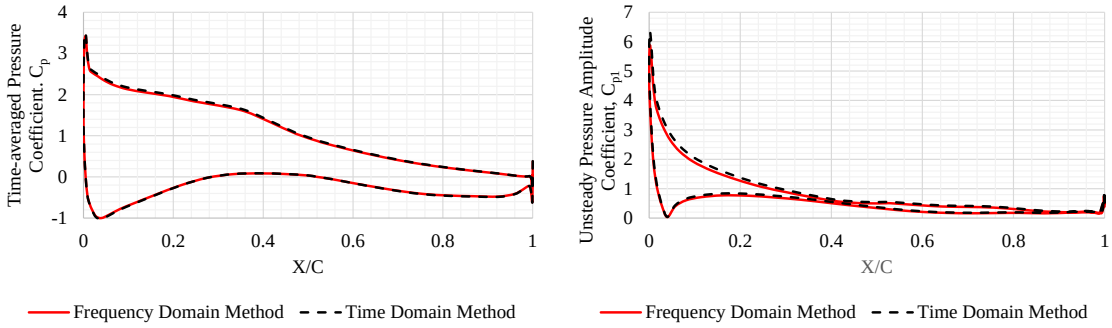

(a) (b)

FIGURE 4: (A) TIME-AVERAGED AND (B) UNSTEADY PRESSURE AMPLITUDE COEFFICIENT DISTRIBUTIONS AT 30%SPAN

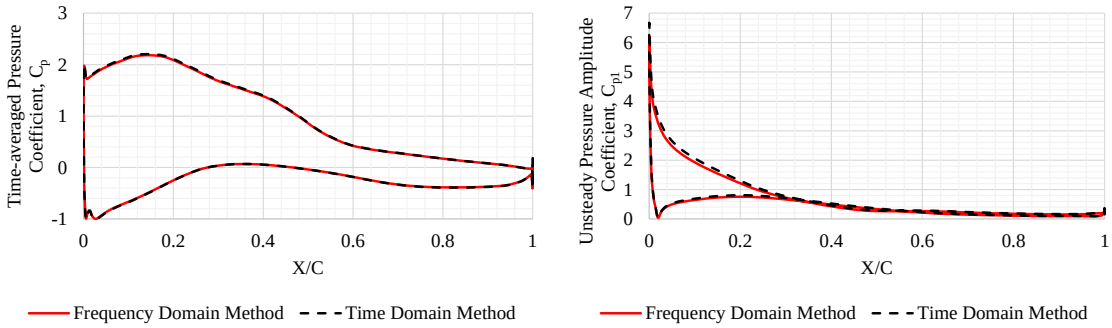

(a) (b)

FIGURE 5: (A) TIME-AVERAGED AND (B) UNSTEADY PRESSURE AMPLITUDE COEFFICIENT DISTRIBUTIONS AT 50%SPAN

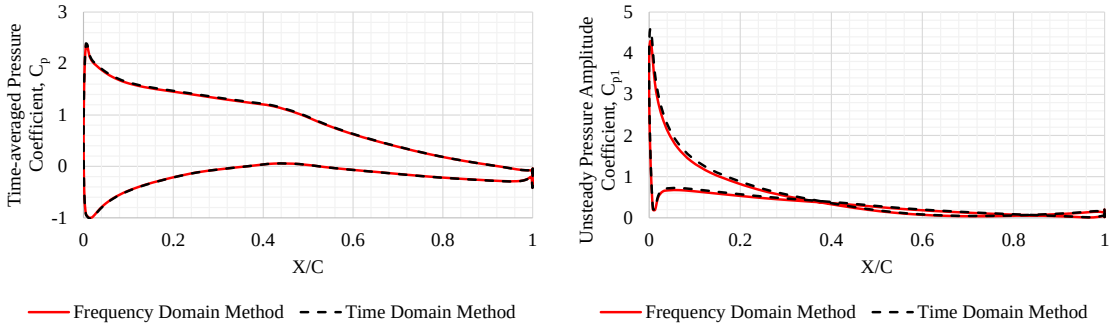

(a) (b)

FIGURE 6: (A) TIME-AVERAGED AND (B) UNSTEADY PRESSURE AMPLITUDE COEFFICIENT DISTRIBUTIONS AT 90%SPAN

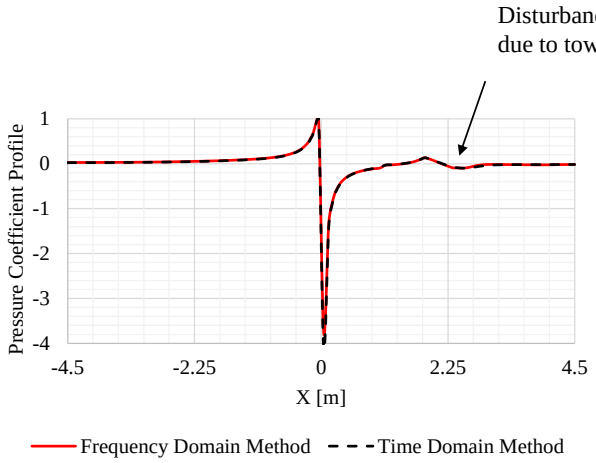

FIGURE 7: PRESSURE COEFFICIENT PROFILE *('0' MARKS THE ROTOR PLANE; NEGATIVE AXIS AND POSITIVE AXIS REPRESENT UPSTREAM AND DOWNSTREAM OF THE ROTOR, RESPECTIVELY)*

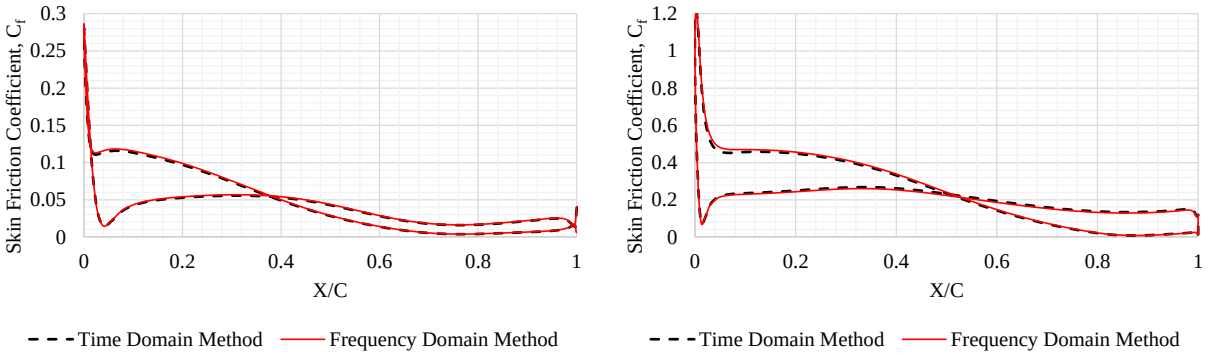

(a) (b)

FIGURE 8: SKIN FRICTION COEFFICIENTS AT (A) 30% AND (B) 90% SPAN BLADE SECTIONS

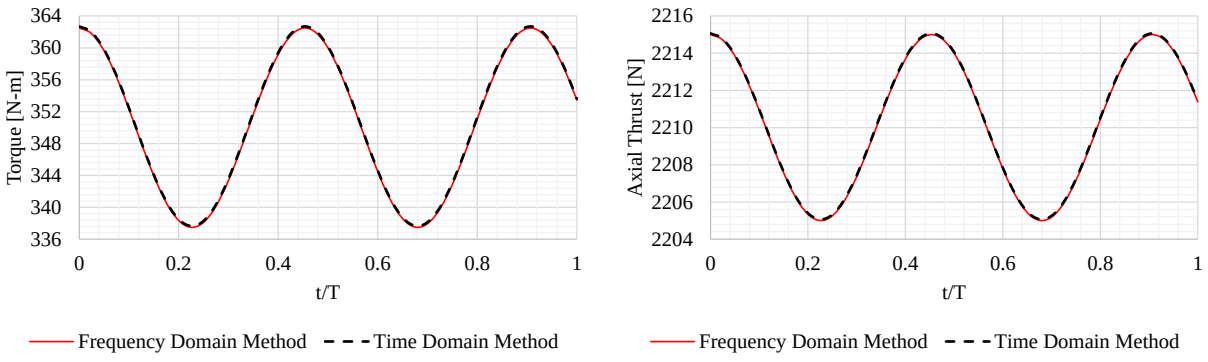

(a)

(b)

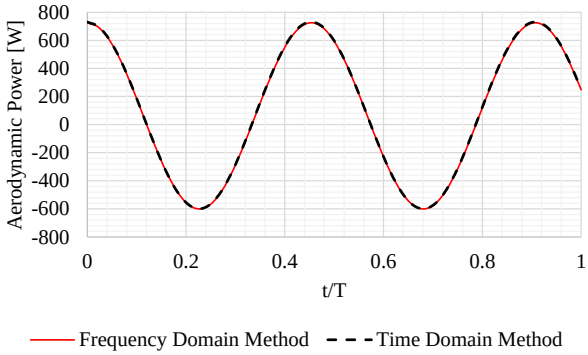

(c)

FIGURE 9: (A) TORQUE, (B) AXIAL THRUST, AND (C) AERODYNAMIC POWER PROFILES

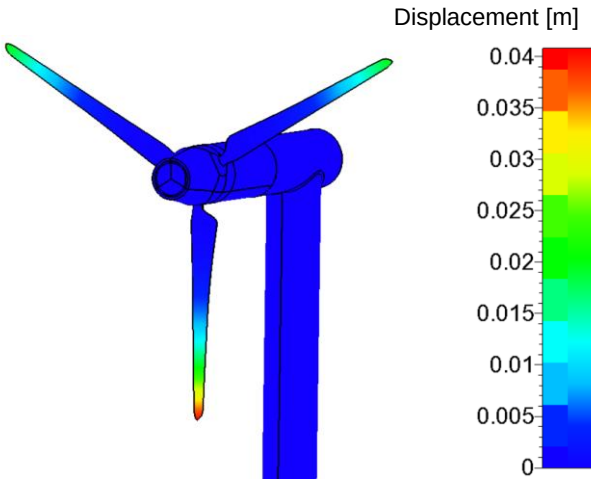

FIGURE 10: DISPLACEMENT CONTOUR

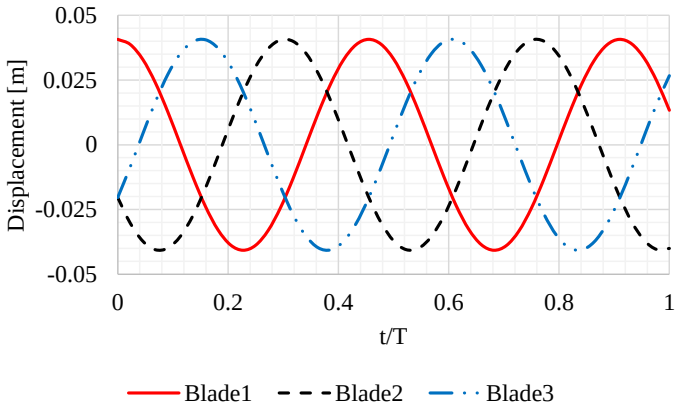

FIGURE 11: DISPLACEMENT PROFILES *(BLADE 1 REPRESENTS THE ONE AT SIX O'CLOCK POSITION. POSITIVE AND NEGATIVE VALUES OF DISPLACEMENT REPRESENT BLADE DEFLECTING BACKWARDS AND FORWARD, RESPECTIVELY)*

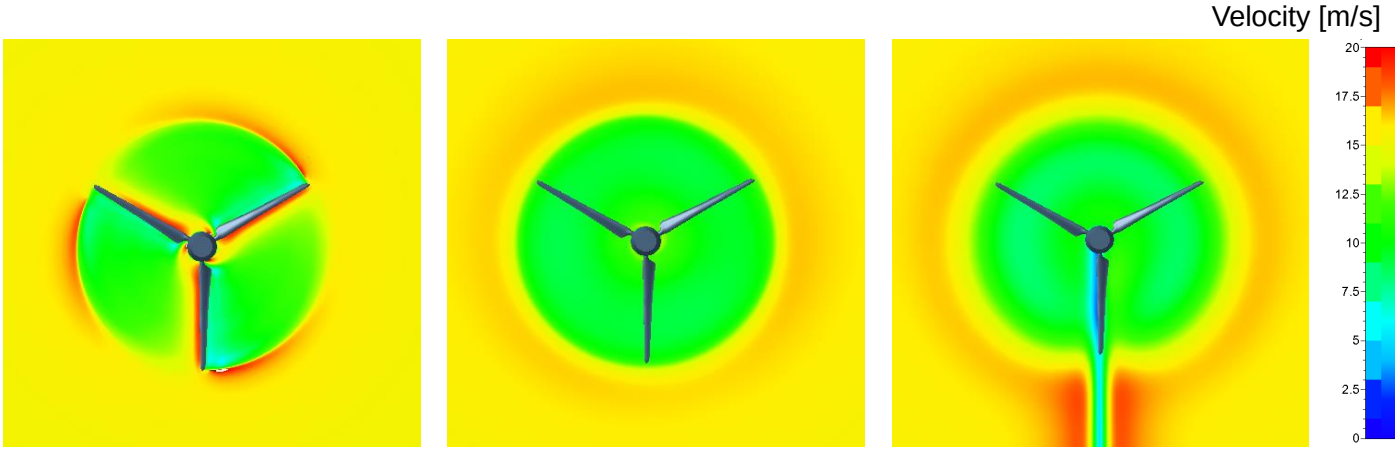

(a) (b) (c)

FIGURE 12: VELOCITY FIELDS ON THE PLANE (A) JUST BEHIND THE ROTOR, (B) AT THE MIDDLE BETWEEN THE ROTOR AND THE TOWER, AND (C) JUST BEFORE THE TOWER

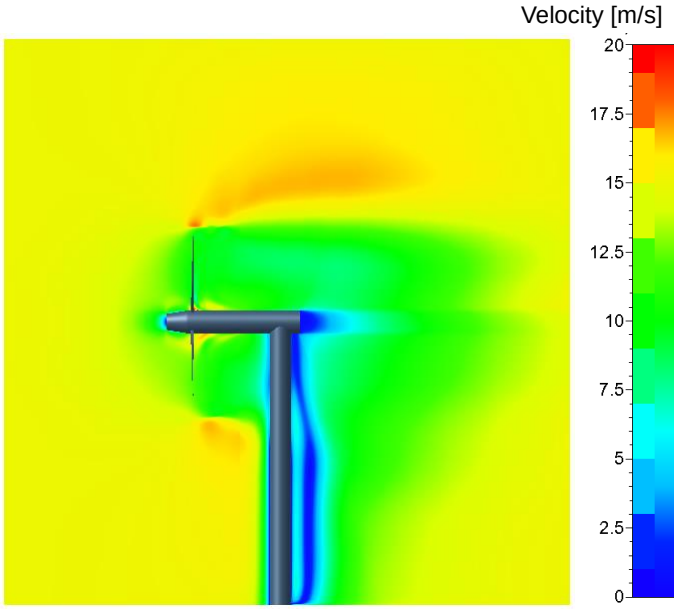

FIGURE 13: VELOCITY FIELDS IN THE MERIDIONAL VIEW